Hindawi
Journal of Chemistry
Volume 2023, Article ID 2554098, 12 pages
https://doi.org/10.1155/2023/2554098

Research Article

Study of Microstructure and Wear Resistance of AA5052/B_4C Nanocomposites as a Function of Volume Fraction Reinforcement to Particle Size Ratio by ANN

D. Dinesh Kumar,[1] A. Balamurugan,[2] K. C. Suresh,[3] R. Suresh Kumar,[4] N. Jayanthi,[5] T. Ramakrishnan,[6] S. K. Hasane Ahammad,[7] S. Mayakannan,[8] and S. Venkatesa Prabhu[9]

[1]*Department of Electronics and Instrumentation Engineering, St. Joseph's College of Engineering, OMR Road, Chennai, Tamilnadu, India*
[2]*Department of Physics, Government Arts and Science College, Avinashi, Tamil Nadu, India*
[3]*Department of Physics, Government First Grade Women's College, Tumkur, Karnataka, India*
[4]*Department of Mechanical Engineering, R. M. K. Engineering College, Chennai, Tamilnadu, India*
[5]*Department of Physics, R. M. K College of Engineering and Technology, Chennai, Tamilnadu, India*
[6]*Department of Mechanical Engineering, Sri Eshwar College of Engineering, Coimbatore, Tamilnadu, India*
[7]*Department of Electronics and Communication Engineering, Koneru Lakshmaiah Education Foundation, Guntur, Andhra Pradesh, India*
[8]*Department of Mechanical Engineering, Vidyaa Vikas College of Engineering and Technology, Tiruchengode, Namakkal, Tamilnadu, India*
[9]*Center of Excellence for Bioprocess and Biotechnology, Department of Chemical Engineering, College of Biological and Chemical Engineering, Addis Ababa Science and Technology University, Addis Ababa, Ethiopia*

Correspondence should be addressed to S. Venkatesa Prabhu; venkatesa.prabhu@aastu.edu.et

Received 14 October 2022; Revised 29 January 2023; Accepted 5 April 2023; Published 18 April 2023

Academic Editor: B. R. Ramesh Bapu

The effects of the percentage volume of reinforcement, the ratio of reinforcement, and the matrix size of particles on the wear behavior of AA5052/B_4C metal matrix composites (MMCs) examine. This research examines a model function developed from an artificial neural network (ANN). AA5052/B_4C composites bent using a powder metallurgy technique to hardness and ball-on-disc wear testing. There are two exemptions such as (1) when the percentage volume of reinforcement is less than 8% and (2) when the ratio of reinforcement particle size (Rs) and matrix particle size (Ms) increases before decreasing. The results show that wear loss decreases with increasing percentage volume of reinforcement and ratio of Rs and Ms. In the second case, wear loss is increased at high levels of percentage volume (14%) since the proportion of reinforcement and matrix size of the particle is close to 1. When the volume percentage of reinforcement is high (14%) and the matrix and reinforcement particle sizes are substantial (120 m), the reinforcement particles become dislodged and break. Because these broken-up particles are easily removed from the surface, the material's wear resistance is reduced. In this case, raising the volume fraction yields a uniformly higher hardness for all Rs/Ms values; hence, composites with lower reinforcement volume percentages show better wear resistance. Hardness and wear resistance have no relationship with one another.

1. Introduction

MMCs are an emerging material class with a wide range of desirable properties, including low weight, high strength, specific modulus, low density, low elongation, and high stiffness [1]. Excellent operating performance, wear resistance, thermal stabilization, minimal thermal extension, and maximum flexibility to experience the distortion process by conventional methods such as powder metallurgy and casting have contributed to the increase in emerging of AMMC strengthened with ceramics in both the industry and academia. As a result of its compatibility with a wide variety of metallic and ceramic substrate plating materials, AA5052/B_4Cp is useful in microelectronic packing for aviation, automation, and microapplications.

Because of its unique qualities, including the lack of undesired reaction products and less processing cost, solid-state powder metallurgy (PM) is frequently employed as a production method for Al-based MMCs [2, 3]. However, this approach also has drawbacks, such as a lack of homogeneity and a low density from the pores [4].

Sintering, pressing, mixing settings (external factors), and material aspects all influence the qualities of particulate-reinforced MMCs made through solid-state powder metallurgy. Material factors (internal factors) considered in this investigation include Ms and Rs and the percentage volume of reinforcement particles.

Wear resistance in Al-based MMCs has been found to increase with both Rs and volume percentage of reinforcement [5]. Although internal parameters have a significant bearing on tribological features and reinforcement particle clustering, the impact of the matrix size of the particle and the ratio of Rs/Ms has not been extensively studied.

Analysts frequently resort to analytical approaches to investigate the effects of MMCs' material features [6]. The use of an ANN is currently one of the most widely adopted and successful approaches. Characterizing the material and providing insight into the effective manufacturing material and processing parameters are two additional benefits of using ANN [7]. Thickness, porous, and stiffness predictions for AA5052/B_4C MMC were investigated by authors [8]. Their analysis took a Cu-weight percentage and a B_4C volume fraction as input parameters. A maximum inaccuracy of 5.99% was determined.

Researchers [9]employed an artificial neural network to examine the relationship between the axial stress and strain of AA5052/B_4Cp MMCs and the thickness, size of the particle, percentage volume of particles, and load. The authors [10] also used an artificial neural network to examine the results of particle size, percentage of volume, and milling duration on the density, hardness, and tensile strength of Al2024/B_4C MMCs. The authors examined the bending strength and stiffness of aluminium-silicon-magnesium-based MMC [11] using ANN to see if they varied with the Rs. The B_4C particle was the only input during ANN. Researchers found that B_4C's hardness and bending strength improved along with its particle size [11].

The wear resistance of MMCs was studied using ANN in specific research. To examine wear behavior, authors [12] used ANN on AA5052/B_4C MMCs. The wear behavior of AA5052/B_4C MMCs was studied to determine the impact of load and testing temperature. At the same time, in investigating the wear rate of aluminium/Al_2O_3 MMCs, authors [13] employed an ANN technique, with a wear rate as output and percentage volume of reinforcement, applying pressure, sliding speed, and testing temperature as input factors. Clustering, an undesirable phenomenon, is reported to increase the volume percentage of reinforcement. Authors [14] also investigated the impact of the reinforcing volume fraction. The researchers discovered that squeeze-cast AA5052/B_4C MMCs with a higher volume proportion of B_4C particles had better wear resistance [15–17]. They also found that an increase in percentage volume led to a higher critical transition temperature between the moderate and severe regimes of wear loss [17]. Additional instances of the successful application of ANN to the characterization of MMCs can be found in the scholarly literature [18].

This research looked at how the Rs/Ms ratio affected the wear behavior of AA5052/B_4Cp MMCs. The studies relied on a model function determined with the help of a neural network simulator and the data collected in the experiments. Micrographs of the microstructures were acquired before and after the wear testing, allowing for a comparison of the two data sets. To get a more in-depth look at AA5052/B_4Cp MMCs to wear, an ANN was used with wear loss and hardness as input factors and percentage volume of reinforcement, Ms and Rs as output parameters.

2. Materials and Experimental Procedure

Production of AA5052-B_4C composites was achieved through powder metallurgy. Five different volume fractions of B_4C particles were used to strengthen the aluminum particles (99.5% purity). Matrix and reinforcement particle sizes of 70, 95, 120, 145, and 170 μm were tested and found to be optimal. In a triaxial mixer, particles of aluminum and B_4C of varying sizes were mixed for a one-hour cold compact at a pressure 450 MPa. After compacting, the particle mixes were sintered at 600 C for 8 hours.

The hardness of the composite specimen was evaluated using a Brinell hardness tester (DM-AKB-3000, Navin Engineering) outfitted with a ball indenter measuring 2.5 mm in diameter and a 62.5 kgf force. The wear tests were conducted in the ball-on-disc-type machine with dry sliding circumstances. Steel ball bearings with a diameter of 6 mm and a hardness of 62HRC were employed as the counter-face material. Normal loads of 10 N were applied for the wear testing, and the sliding velocity was held constant at 0.421 ms^{-1}, with the sliding distance set at 550 m. The starting and ending weights of every sample were recorded to calculate wear.

Table 1 displays the wear loss and hardness test results for all the specimens tested, including those with a wide variety of matrix particle sizes, reinforcement particle sizes, and reinforcement volume fractions.

Table 1: Data for various process parameters.

Sample no.	Reinforcement volume fraction	Size of reinforcement particle	Size of matrix particle	Rs/Ms proportion	Wear loss	Hardness	Clustering rate
Unit	(%)	(R_s) (μm)	(M_s) (μm)		(g)	(HB)	(%)
1	6	120	120	1.20	0.049891	35.2	No cluster
2	8	95	145	0.75	0.013212	38.3	3.72
3	8	95	95	1.20	0.030286	39.7	2.63
4	8	145	145	1.20	0.025552	37.2	1.98
5	8	145	95	1.80	0.044321	39.3	0.93
6	12	70	120	0.73	0.008251	41.3	9.15
7	12	120	170	0.84	0.003065	42.4	8.06
8	12	120	120	1.20	0.006964	40.8	6.45
9	12	170	120	1.45	0.020632	40.3	4.81
10	12	120	70	1.78	0.027553	39.2	3.93
11	18	95	145	0.75	0.002255	41.6	13.46
12	18	95	95	1.20	0.003668	44.2	8.21
13	18	145	145	1.20	0.002815	40.3	10.81
14	18	145	95	1.74	0.003793	43.1	6.36
15	20	120	120	1.20	0.001894	44.7	15.53

3. Artificial Neural Network

Digital models of the nervous systems and artificial neural networks are based on the biology of intelligence [19]. They are typically depicted as networks of neurons that can calculate values from inputs when data are fed into the system. The ability of artificial neural network models to infer a function from observation is often cited as proof of their usefulness. This is especially helpful when it would be impractical to design such a function by hand, as is the case when working with complex data or tasks. This means that ANNs can provide meaning for the interrelationships between the variables of a high-dimensional space. When asked to represent intricate linear and nonlinear connections, ANNs have excelled well. Compared to statistical approaches, ANNs provide a radically new way to describe materials and manage their processing.

Neural networks can be programmed to do a variety of tasks. The neural network is seen in Figure 1. The weight matrices (w), bias vectors (b), transfer function (f), reinforcement (R), and outputs (a) in this network are R, f, w, and a, respectively.

Training a neural network needs to receive examples of data that may be used as inputs. Each input is multiplied by a variant known as the weight and added to a variant known as the bias beforehand, incoming the neuron; the preliminary range of both variations can be specified in advance if the neural network has only one layer [18]. The experimental output value is compared with the neuron's output, which is the functional transfer input. The input is the total of the values received from each input. If the resulting error value exceeds the allowed error value, the result is sent back to the network to adjust the weights and biases until the intended effect is achieved. Figure 2 depicts the iterative process of network training and evaluation, with various techniques used to explore the resulting model's performance.

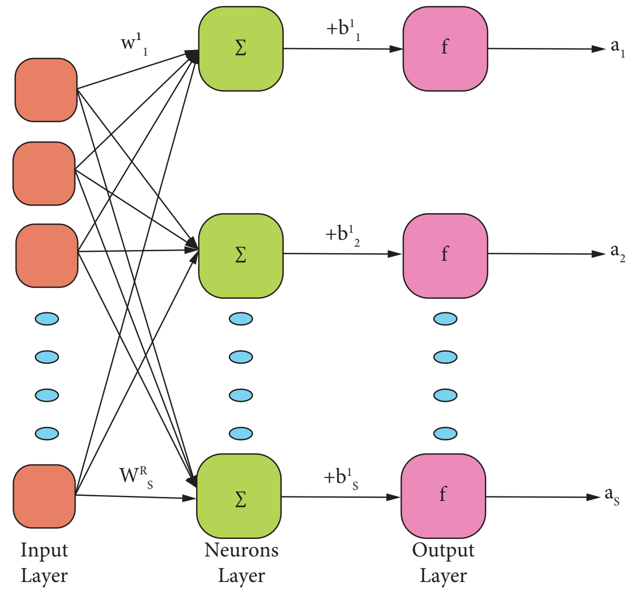

Figure 1: Single layer network with R/S neurons.

3.1. Implementation of the Neural Network. Numerous parameters can be adjusted during installation to optimize the performance, speed, and accuracy of an ANN [20]. Parameters include the network learning rate, the number of layers, the number of neurons in each layer, and many others. In this research, the neural network was trained using abrasive resistance and hardness as input factors and the Rs, Ms, and the reinforcement volume fraction. The network was educated using the most popular and effective approach for training, backpropagation error. According to authors [21], the Pearson correlation coefficient is the other artificial neural network metric that demonstrates how successfully a network is trained. The research shows that Pearson correlation coefficient values greater than 0.9 are considered satisfactory for this parameter [22].

Dispersion in the training data can significantly affect the number of layers and neurons; similarly, variation in the input and output factors might cause difficulties in the network learning process. Data are normalized to reduce the variation in such circumstances. Similar to the method used by authors [23], all parameter values were normalized in this study by dividing them by the most significant value of the relevant parameter to place them in a uniform range from 0 to 1. The optimal PCC (postclassification comparison) value was found by trial and error. Table 2 provides the artificial neural network's specific architecture and the relevant factors' values. There were three distinct layers to the network. The ANN structure gave nominal values for the sum of neurons in the input, hidden, and output layers. Authors [24] indicate that growing the number of neurons, being the minor process units, does not result in enhanced network performance and accuracy. This is something to remember while choosing the number of layers and neurons. The rate at which a network learns is another crucial variable that must be considered during deployment. Authors [25] discussed that a low value for this parameter results in slow network convergence, which slows down the time it takes to obtain the desired response. In that case, there is a risk that the training process may become unstable, increasing the amount of inaccuracy in the response from cycle to cycle.

3.2. Model Function. The values of w, f, p, and b parameters can be acquired upon successful training of the neural network. Figure 3 indicates the overall structure of the neural network used in this research. Using these values, one may determine the function that connects the manufacturing process parameters as inputs to the measured outcomes (wear loss and hardness) as outputs. The model function can be derived as follows:

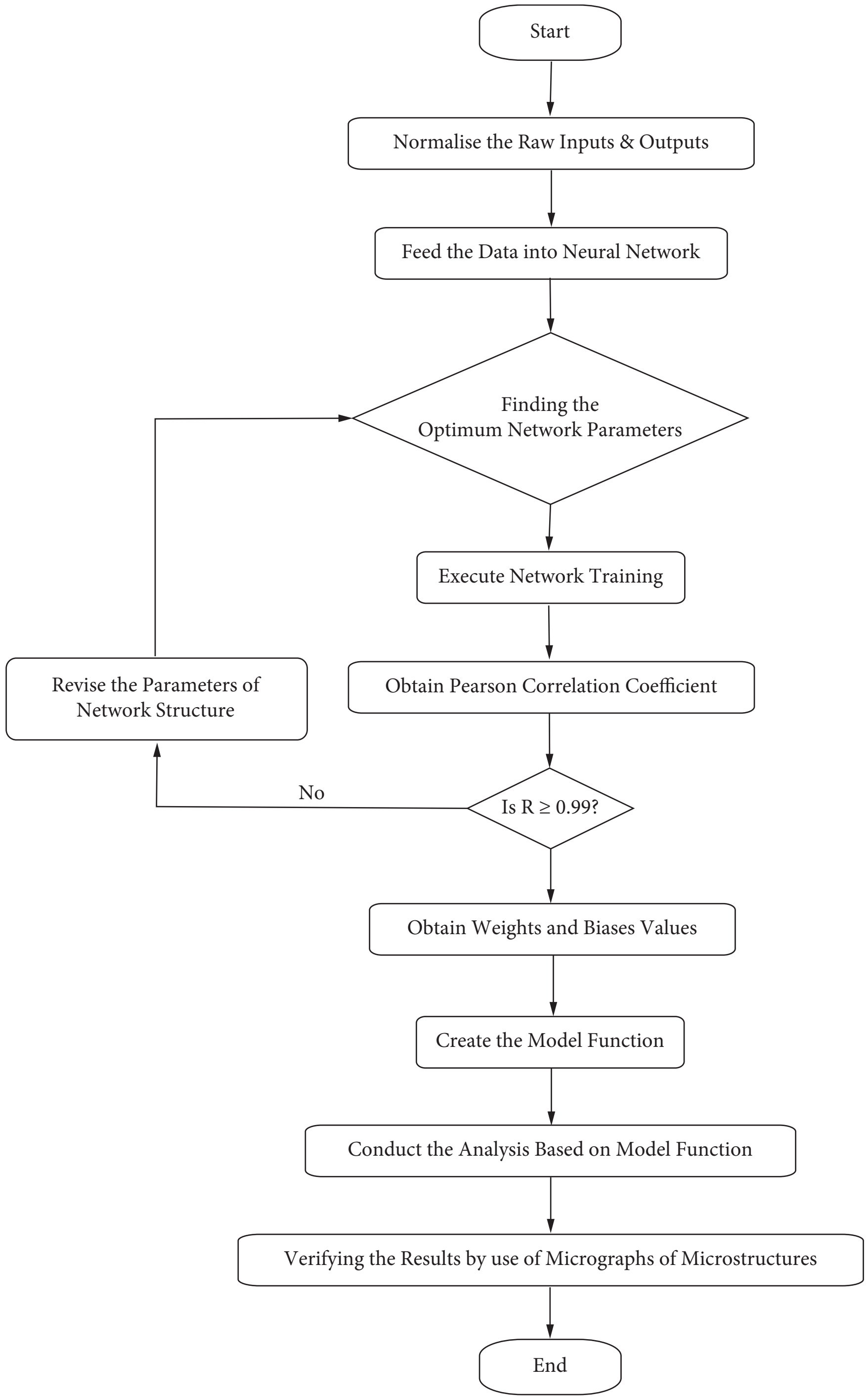

Figure 2: Network training, exploration of ANN training results, and evaluation of result composition of the technique.

Table 2: Assembly and the factors of ANN.

ANN framework	PCC	Rate of learning	Number of epochs	Mean error (%)
$3 \times 8 \times 2$	0.9991	0.094	150000	0.096

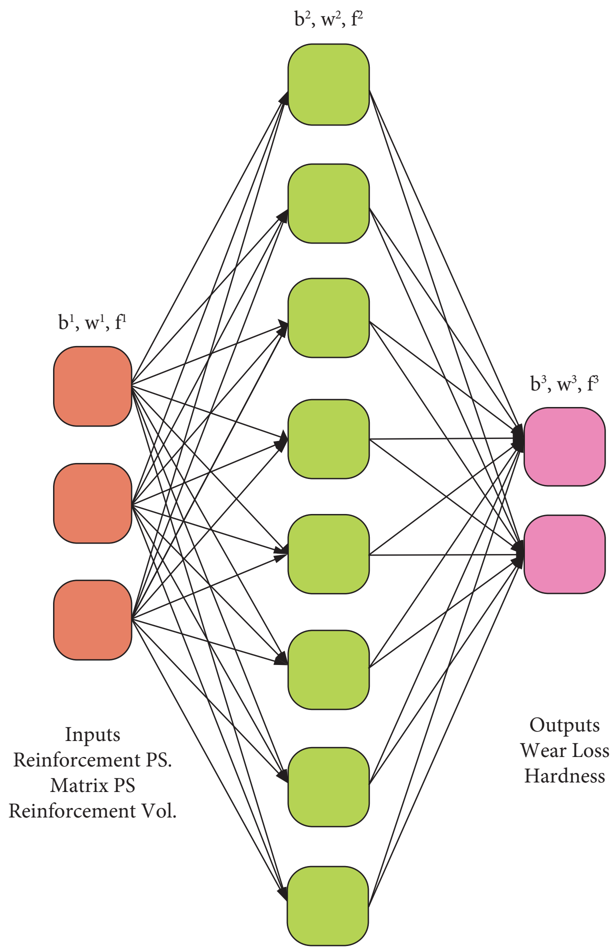

Figure 3: Framework of the functional ANN.

$$\begin{aligned} a^1 &= f^1\left(W^1 p + b^1\right), \\ a^2 &= f^2\left(W^2 a^1 + b^2\right), \\ a^3 &= f^3\left(W^3 a^2 + b^3\right), \\ G(g(1), g(2)) = a^3 &= f^3\left(W^3 f^2\left(W^2 f^1\left(W^1 p + b^1\right) + b^2\right) + b^3\right), \end{aligned} \tag{1}$$

a^3 is the output of the third layer, which is equivalent to the function G ($g(1)$, $g(2)$), and a^1 and a^2 are the outputs of the first and second layers, respectively. $G(g(1)$ and $g(2))$ are the resultant factors for measured values. Ms, Rs is used in the function G to calculate wear loss and hardness.

4. Results and Discussions

4.1. Artificial Neural Network. For wear loss as well as hardness, as can be shown in Figures 4(a) and 4(b), the ANN predictions are close to the experimental results. The ANN model has a 1% margin of error for making predictions (Table 2). This means that the projected findings agree well with the experimented data. The results show that an artificial neural network is a valuable tool for predicting the wear behavior of particle-strengthened MMCs and can be utilized in conjunction with experimental results.

4.2. Analysis of Microstructure. Figure 5 shows the optical microstructures of AA5052-B_4Cp MMCs. Microscopically, 8% volume fraction composites have a homogeneous distribution of reinforcing particles (Figures 5(a) and 5(b)). In these composites, the reinforcement (Rs) and the matrix (Ms) particle size ratio is more than one or equal to 1. While the reinforcement volume percentage is less, Figure 5(c) shows that few particle clusters arise in the microstructure when the reinforcement size is lesser than the matrix size of the particle (Rs/Ms < 1) (8%). However, particle clusters are more numerous in composites with a large volume fraction

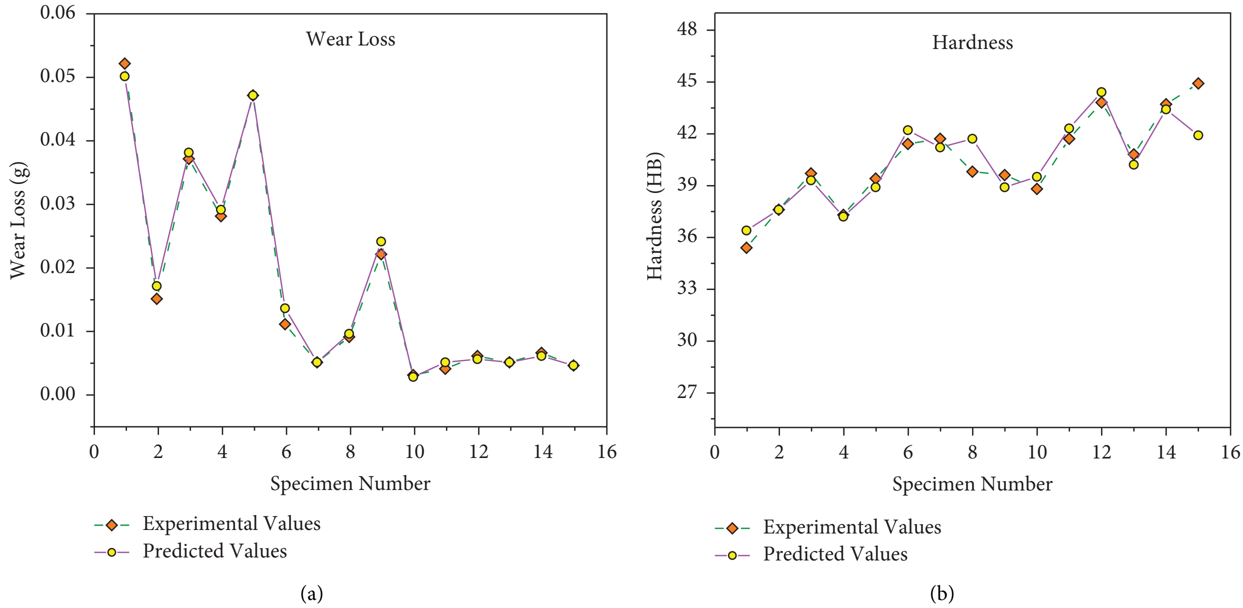

Figure 4: Evaluation of the experimented values and theoretical values (a) wear loss and (b) hardness.

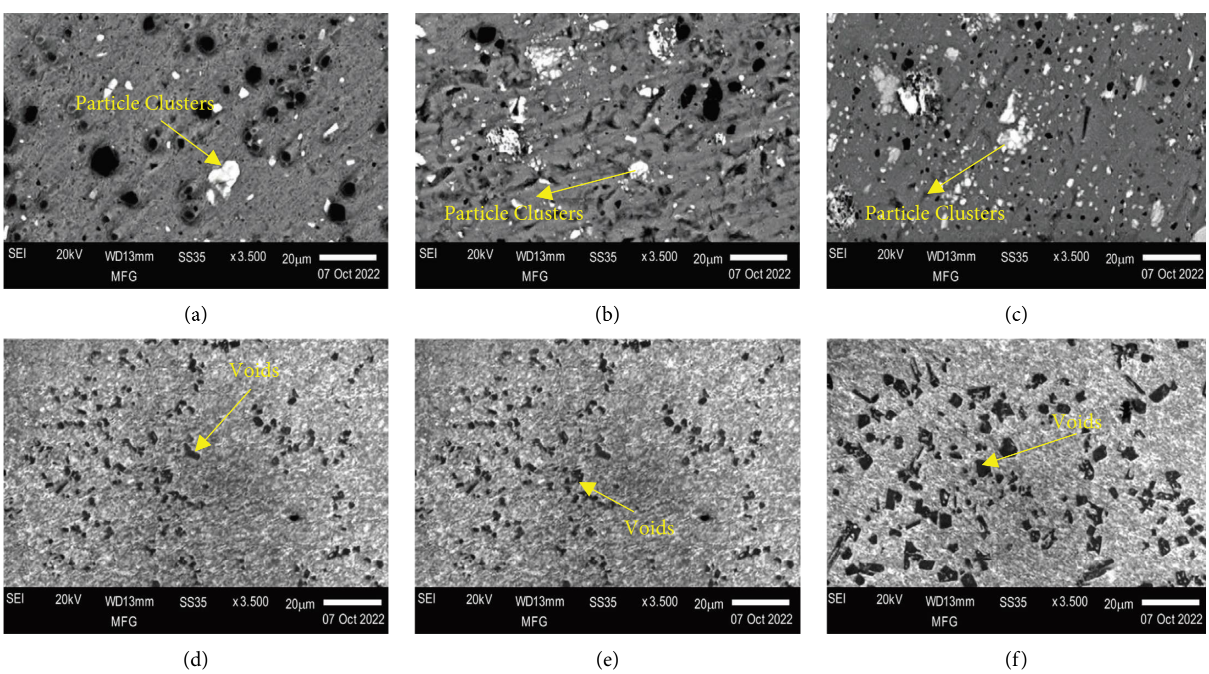

Figure 5: Microstructure images of AA5052-B_4Cp MMCs: (a) 8% AA5052/95-B_4C/145; (b) 8% AA5052/95-B_4C/95; (c) 8% AA5052/95-B_4C/95; (d) 18% AA5052/95-B_4C/145; (e) 18% AA5052/95-B_4C-95; (f) 18% AA5052/145-B_4C/95.

(18%), which is true regardless of the Rs/Ms (Figures 5(d)–5(f)). This research determined the clustering rate of reinforcement particles by comparing the cluster area to the total microstructure area. Seven micrographs were obtained from each sample, the parameter value was determined for each, and the average was used to determine the clustering rate. Comparing only specimens with 18% of reinforcement reveals that the clustering of strengthening particles becomes less severe with an increasing Rs/Ms ratio.

It can also be seen clearly from Table 1 and Figure 5 that when the volume proportion rises and the Rs/Ms ratio falls, the degree of reinforcement particle clustering increases. These findings suggest that reinforcement particles' distribution and cluster formation are controlled by the Rs/Ms ratio in addition to the volume fraction. The dashed arrows represent particle clusters with space in Figure 5. There are two distinct ways these gaps can emerge. Inefficient bonding between the groups of reinforcement particles makes them

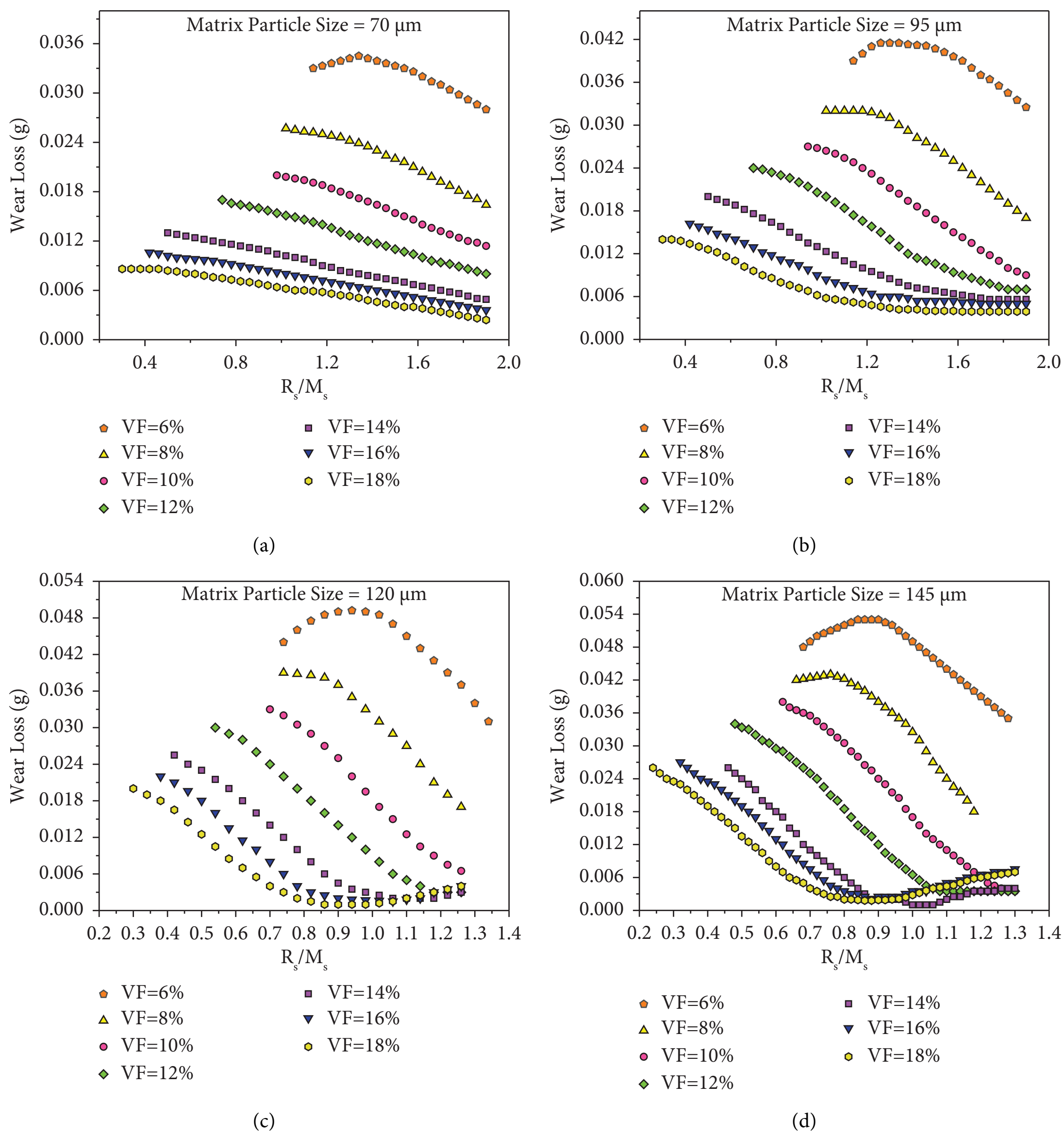

Figure 6: Predicted wear loss for various matrix particle sizes (a) 70 μm, (b) 95 μm, (c) 120 μm, and (d) 145 μm.

easy to dislodge or remove from the matrix. In this case, sliding wear tests have not yet been conducted. Second, when deformed plastically, the matrix material has difficulty filling the gaps between the reinforcement particles. This is because the reinforcing particles are clustered too closely together, which impedes the flow of the matrix material during the pressing and sintering processes. It explains how the reinforcement particle clustering affects the AA5052/B_4Cp MMCs' wear behavior.

4.3. Wear Behavior. Figure 6 shows that AA5052/B_4Cp composites' wear behavior is affected by reinforcement volume percentage and the Rs/Ms factors. The percentage of reinforcement volume in a material's total volume is essential in determining its wear resistance. As the volume fraction of reinforcement rises, wear loss falls. However, as seen in Figures 6(a)–6(d), wear loss rises with the increasing matrix size of the particle. The impact of particle size reinforcement on wear resistance is complex and cannot be analyzed in isolation. Once the strengthening volume percentage is more significant than 12% and the Rs is less than half that of the Ms (Rs/Ms 0.5), the wear loss appears to decrease slightly. However, wear loss starts to diminish as the relative Rs increases drastically. There is a minimum in the wear loss's lowering trend at high reinforcement volume fraction and Rs, which then starts to climb again. The wear behavior of AA5052/B_4Cp MMCs can be better examined and comprehended if a second parameter is defined to account for the size of the reinforcement particles. This study developed a new metric, Rs/Ms, to accomplish this.

The model function (Figure 6, Table 1) and experimented data show wear loss reductions as the ratio of Rs and Ms increases. Previously established, this ratio demonstrates

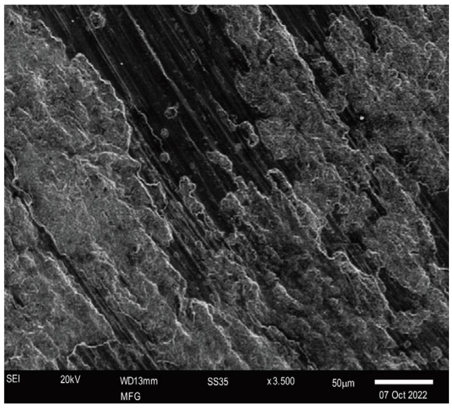

(a)

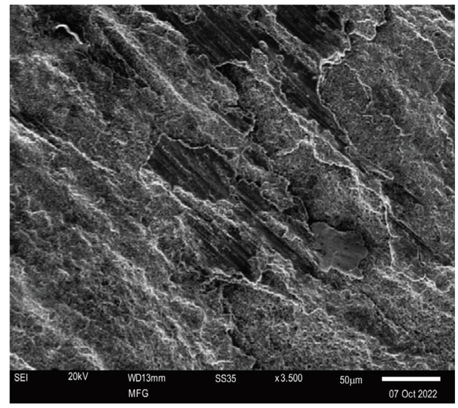

(b)

Figure 7: SEM morphologies of worn surfaces of (a) 8% AA5052/145-B_4C95 μm and (b) 18% AA5052/145-B_4C/145 μm.

how many reinforcement particles there are for every hundred matrix particles [26]. As the mixture is stirred, the smaller matrix particles can more effectively fill the spaces between the larger reinforcement particles. Wear resistance improves as the ratio of Rs/Ms increases. With just two exceptions, wear loss reduces with increasing Rs/Ms. In the first scenario, the volume fraction is between 6 and 8%. As shown in Figure 6, the wear rate decreases after reaching a maximum. In this second scenario, the volume percentage of reinforcement is more than 14%, the reinforcement and matrix particle size proportion is close to 1, and the matrix particle size is more than 120 μm. When the particle size of the matrix increases, the wear loss falls until a minimum is attained, and then the minimum moves to a lesser range of the ratio of Rs and Ms (Figures 6(c) and 6(d)).

Figure 7(a) demonstrates that the reinforcement particles cannot prevent substantial plastic distortion in the first situation, while the sample surface is in metal-metal contact when the testing load is relatively high. Larger reinforcement particles induce extensive plastic deformation and wear loss, which may be attributed to their poorer strength due to harboring more defects, as observed by authors [27, 28]. In addition, low Rs/Ms can cause particle clusters, resulting in a significant amount of wear loss. But after wear loss has plateaued at a given reinforcing particle size, further increases in particle size reduce the rate of wear (Figure 6). Because larger reinforcement particles are lodged so profoundly in the matrix, they are better able to shield the matrix from damage and hence prevent the plastic distortion of the specimen's surface.

As shown in Figure 5, the volume proportion of reinforcement particles and the number of particle clusters raise the reinforcement and matrix size particle ratio to a specific fixed maximum value of volume percentage. Authors [29–31] conducted a few other study teams that have come to similar conclusions. Wear loss decreases initially despite an increase in Rs/Ms in another case when the percentage volume of reinforcement is more significant than 14% and the Ms is > 120 μm (Figures 6(c) and 6(d)). A maximum volume proportion of reinforcement (>14%) is responsible for the

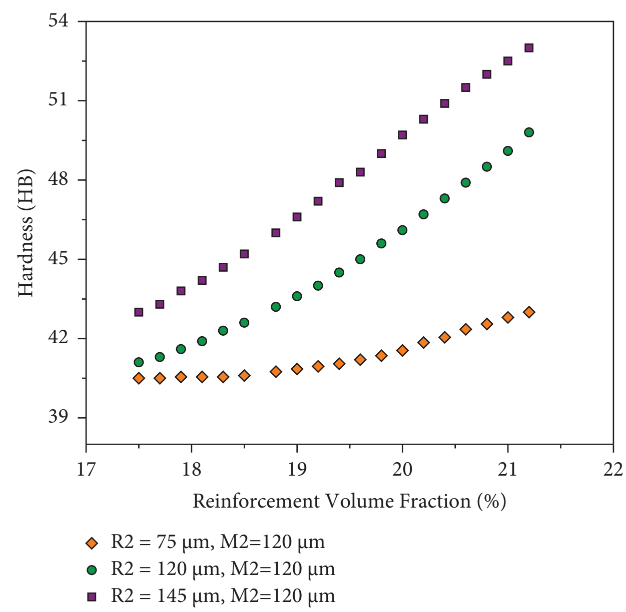

Figure 8: Composites with varied Rs/Ms ratios with varying hardness.

observed upward trend in wear loss. The minimum process temperature of the MMC prevents diffusion between the B_4C and AA5052 particles, resulting in weak bonding in the clustered particles that make up the microstructure of MMCs [32, 33]. Because of this, particles are easily knocked off the sample's surfaces during the wear test [34]. The spaces left behind by considerable dislodged particles are not always filled. Depending on the particle cluster, the voids created in the present investigation may be noticed in Figure 5 well before the wear test was performed. As shown in Figure 7(b), the wear loss increases because the dislodged particles become imprisoned among the sample surface and counter-face, breaking apart (Figures 6(c) and 6(d)). When the percentage volume of reinforcement (14%) and the percentage volume of the matrix (120 μm) are both high, the high Rs/Ms cannot improve the wear resistance of MMCs.

4.4. Hardness. Hardness increases with increasing volume fraction, as demonstrated by investigations by the authors [35–37]. Dislodging and fracturing of reinforcing particles diminish wear resistance, as seen in Figure 8. In contrast to the wear loss trends, which show an increase as a function of rising volume fraction, it is clear that hardness improves for all ranges of Rs/Ms. This suggests an inverse relationship between hardness and wear resistance in this region.

5. Conclusions

Using a numerical model derived from a trained ANN, this research examined the wear resistance as well as hardness of AA5052/B_4Cp metal matrix composites and found the following:

(1) Percentage volume of reinforcement, followed by the ratio of particle size reinforcement to particle size matrix, is the essential factor in defining the wear resistance of AA5052/B_4Cp MMCs, and more accurate results can be obtained

(2) Except in two situations, wear resistance improves with an increase in the Rs/Ms ratio: for (a), the reinforcement volume fraction must be less than 8%. Here, (a) the percentage volume is greater than 14%, (b) the Rs/Ms is close to 1, and (c) the Ms is more significant than 120 μm; wear loss diminishes as the Rs/Ms ratio increases. The lost wear reduces until it reaches a minimum and then rises again.

(3) Reinforcing particle clustering has a significant impact on wear loss. The wear resistance goes down with the number of clusters. The proportion of reinforcement volume to particle volume and the strengthening stiffness to particle stiffness are essential factors in particle clustering. Wear resistance is inversely proportional to the Rs/Ms ratio, which means that raising the volume percentage increases the particle clustering.

(4) The reinforcement particles become dislodged and break when the volume percentage of reinforcement is high (14%) and when the particle sizes of both the reinforcement and the matrix are significant (120 μm). The material's wear resistance is decreased because these fragmented particles can be readily cleaned off the surface. Here, increasing the volume fraction results in a greater hardness across the board for all Rs/Ms values; hence, composites with lower reinforcement volume percentages exhibit more excellent wear resistance. There is no correlation between wear resistance and hardness.

(5) Through the use of a qualified ANN, the wear behavior of particle-reinforced metal matrix composites was successfully characterized for the first time. The network took as input parameters the particle size and volume fraction of the reinforcement in the matrix, and the network output factors were the wear loss and hardness of the composite.

Data Availability

All data supporting the findings of this study are included within the manuscript.

Ethical Approval

All procedures performed in this study involving human participants were by the ethical standards of the institutional and/or national research committee and its later amendments or comparable ethical standards.

Disclosure

The funders had no role in the study design, data collection, and analysis, publication decision, or manuscript preparation.

Conflicts of Interest

The authors declare that they have no conflicts of interest.

References

[1] M. Patel, M. K. Singh, and S. K. Sahu, "Abrasive wear behaviour of sand cast B4C particulate reinforced AA5052 metal matrix composite," in *Innovative Product Design and Intelligent Manufacturing Systems*, B. Deepak, D. Parhi, and P. Jena, Eds., Springer, Singapore, pp. 359–369, 2020.

[2] Q. T. Pham, "A machine learning–based methodology for identification of the plastic flow in aluminum sheets during incremental sheet forming processes," *International Journal of Advanced Manufacturing Technology*, vol. 120, no. 5–6, pp. 3559–3584, 2022.

[3] B. Girinath and N. S. Shanmugam, "A modified version of MATLAB application window for predicting the weld bead profile and stress–strain plot of AA5052 CMT weldment using ER4043," *Simulation*, vol. 98, no. 3, pp. 221–234, 2022.

[4] A. Mulay, B. S. Ben, S. Ismail, and A. Kocanda, "Prediction of average surface roughness and formability in single point incremental forming using artificial neural network," *Archives of Civil and Mechanical Engineering*, vol. 19, no. 4, pp. 1135–1149, 2019.

[5] S. S. Panicker, K. S. Prasad, S. Basak, and S. K. Panda, "Constitutive behavior and deep drawability of three aluminum alloys under different temperatures and deformation speeds," *Journal of Materials Engineering and Performance*, vol. 26, no. 8, pp. 3954–3969, 2017.

[6] B. N. Guniputi, P. R. T, and V. K. Mamidi, "Effect of in-situ reaction time on the strength of AA5052/ZrAl3 metal matrix nanocomposites," *Advances in Materials and Processing Technologies*, pp. 1–12, 2022.

[7] Z. J. Kadhim, H. J. M. Alalkawi, and A. H. Reja, "Evaluation the magnetic and microstructure properties of Al/TiO2nanocomposites using various stir casting temperature," *Journal of Physics: Conference Series*, vol. 1973, no. 1, Article ID 012115, 2021.

[8] F. Khodabakhshi, M. Nosko, and A. P. Gerlich, "Effects of graphene nano-platelets (GNPs) on the microstructural characteristics and textural development of an Al-Mg alloy during friction-stir processing," *Surface and Coatings Technology*, vol. 335, pp. 288–305, 2018.

[9] F. Khodabakhshi, S. M. Arab, P. Švec, and A. P. Gerlich, "Fabrication of a new Al-Mg/graphene nanocomposite by multi-pass friction-stir processing: dispersion, microstructure, stability, and strengthening," *Materials Characterization*, vol. 132, pp. 92–107, 2017.

[10] M. Bodaghi and K. Dehghani, "Friction stir welding of AA5052: the effects of SiC nano-particles addition," *International Journal of Advanced Manufacturing Technology*, vol. 88, no. 9–12, pp. 2651–2660, 2017.

[11] F. Khodabakhshi, A. Simchi, A. H. Kokabi, and A. P. Gerlich, "Friction stir processing of an aluminum-magnesium alloy with pre-placing elemental titanium powder: in-situ formation of an Al3Ti-reinforced nanocomposite and materials characterization," *Materials Characterization*, vol. 108, pp. 102–114, 2015.

[12] B. N. Sharath, C. V. Venkatesh, A. Afzal et al., "Multi ceramic particles inclusion in the Aluminium matrix and wear characterization through experimental and response surface-artificial neural networks," *Materials*, vol. 14, pp. 2895–2911, 2021.

[13] B. N. Sharath, C. Venkatesh, A. Afzal, M. Ahmed Ali Baig, and A. Praveen Kumar, "Study on effect of ceramics on dry sliding wear behaviour of Al-Cu-Mg based metal matrix composite at different temperature," *Materials Today: Proceedings*, vol. 46, pp. 8723–8733, 2021.

[14] K. Trinath, R. Aepuru, A. Biswas, M. Ramalinga Viswanathan, and R. Manu, "Study of self-lubrication property of Al/SiC/Graphite hybrid composite during Machining by using artificial neural networks (ANN)," *Materials Today: Proceedings*, vol. 44, pp. 3881–3887, 2021.

[15] V. Jagota and R. K. Sharma, "Wear volume prediction of AISI H13 die steel using response surface methodology and artificial neural network," *Journal of Mechanical Engineering and Sciences*, vol. 14, no. 2, pp. 6789–6800, 2020.

[16] T. K. Kandavel, T. Ashok Kumar, and E. Varamban, "Prediction of tribological characteristics of powder metallurgy Ti and w added low alloy steels using artificial neural network," *Indian Journal of Engineering and Materials Sciences*, vol. 27, no. 3, pp. 503–517, 2020.

[17] X. Qi, Y. Wang, C. Wang, and R. Zhang, "Microstructure and performance of nano-WC particle-strengthened Ni coatings by electro-brush plating," *Journal of Materials Engineering and Performance*, vol. 27, no. 11, pp. 6069–6079, 2018.

[18] F. B. Marin, M. Marin, G. Gurău, C. Gurău, and A. Petrică, "Application of an artificial neural network for prediction of the wear resistance of sintered iron alloys," *SGEM International Multidisciplinary Scientific GeoConference EXPO Proceedings*, vol. 18, no. 1, pp. 55–60, 2018.

[19] S. Kim, J. Hong, Y. Joo, and M. Kang, "Synergistic effect of SiC nano-reinforcement and vibrator assistance in micro-friction stir welding of dissimilar AA5052-H32/AA6061-T6," *Journal of Manufacturing Processes*, vol. 82, pp. 860–869, 2022.

[20] N. A. Liyakat and D. Veeman, "Improvement of mechanical and microstructural properties of AA 5052-H32 TIG weldment using friction stir processing approach," *Journal of Materials Research and Technology*, vol. 19, pp. 332–344, 2022.

[21] P. Samal, P. R. Vundavilli, A. Meher, and M. M. Mahapatra, "Reinforcing effect of multi-walled carbon nanotubes on microstructure and mechanical behavior of AA5052 composites assisted by in-situ TiC particles," *Ceramics International*, vol. 48, no. 6, pp. 8245–8257, 2022.

[22] J.-W. Choi, W. Li, K. Ushioda, M. Yamamoto, and H. Fujii, "Microstructure evolution and hardness distribution of linear friction welded AA5052-H34 joint and AA5083-O joint," *Journal of Materials Research and Technology*, vol. 17, pp. 2419–2430, 2022.

[23] J. Sarvaiya and D. Singh, "Influence of hybrid pin profile on enhancing microstructure and mechanical properties of AA5052/SiC surface composites fabricated via friction stir processing," *Canadian Metallurgical Quarterly*, pp. 1–14, 2022.

[24] J. T. Chinna Rao, V. Harikiran, K. S. S. Gurudatta, and M. V. D. Kumar Raju, "Temperature and strain distribution during friction stir welding of AA6061 and AA5052 aluminum alloy using deform 3D," *Materials Today: Proceedings*, vol. 59, pp. 576–582, 2022.

[25] S. H. Jo, B. B. Park, and S. H. Lee, "Microstructure and mechanical properties of cold roll-bonded layered aa6061/aa5052/aa6061/aa5052 aluminum alloy sheet," *Korean Journal of Materials Research*, vol. 32, no. 3, pp. 161–167, 2022.

[26] S.-H. Jo and S.-H. Lee, "Microstructural evolution of a cold roll-bonded multi-layer complex aluminum sheet with annealing," *Korean Journal of Materials Research*, vol. 32, no. 2, pp. 72–79, 2022.

[27] P. K. Arya, N. K. Jain, and M. Jayaprakash, "Optimization of process parameters for friction stir welding of Aluminium alloy AA5052-H32 by using taguchi method," *Springer Proceedings in Materials*, vol. 12, pp. 71–81, 2022.

[28] X.-Q. Ren, C. Chen, X.-K. Ran, Y.-X. Li, and X.-G. Zhang, "Microstructure evolution of AA5052 joint failure process and mechanical performance after reconditioning with tubular rivet," *Transactions of Nonferrous Metals Society of China*, vol. 31, no. 11, pp. 3380–3393, 2021.

[29] A. Rajesh Kannan, S. Mohan Kumar, R. Pramod, N. Siva Shanmugam, Y. Palguna, and M. Vishnukumar, "Microstructure and mechanical properties of dissimilar aluminum alloys AA5052-H32 and aa2219-T31 welded using cold metal transfer process," *Materials Performance and Characterization*, vol. 10, no. 1, pp. 20210043–20210657, 2021.

[30] Y. Sai Ratnakar, P. Srinivasa Reddy, M. Gangadhar Rao, and D. Appanna, "Experimental investigation and optimization on microstructure & mechanical properties of AA5052 in comparison with AA2024 and AA8090 using friction stir welding," *International Journal of Performability Engineering*, vol. 17, no. 8, pp. 686–694, 2021.

[31] Z. Chang, M. Yang, and J. Chen, "Experimental investigations on deformation characteristics in microstructure level during incremental forming of AA5052 sheet," *Journal of Materials Processing Technology*, vol. 291, Article ID 117006, 2021.

[32] B. M. Nagarajan and M. Manoharan, "Influence of cooling conditions on tensile lap shear strength and microstructure of friction stir welded aluminum alloy 5052-H32 and polycarbonate light weight hybrid joint," *Journal of Manufacturing Processes*, vol. 82, pp. 390–402, 2022.

[33] L. Song, Z. Xie, H. Gao, C. Kong, and H. Yu, "Microstructure and mechanical properties of ARB-processed AA1050/AA5052 multi-layer laminate sheets during cryorolling," *Materials Letters*, vol. 307, Article ID 130998, 2022.

[34] J. Das, P. S. Robi, and P. K. Sahu, "Influence of process parameters on mechanical and microstructural properties of friction stir welded AA5052," *Advances in Materials and Processing Technologies*, pp. 1–17, 2022.

[35] H. Zhou, P. Yao, Y. Xiao et al., "High energy braking behaviors and tribo-map constructions of Cu metal matrix composites with different Cr volume contents," *Wear*, vol. 496–497, Article ID 204275, 2022.
[36] A. B. Kheradmand, M. R. Fattahi, M. Tayebi, and B. Hamawandi, "Tribological characterization of reinforced Fe matrix composites with hybrid reinforcement of C, Cu, and SiC particulates," *Crystals*, vol. 12, no. 5, p. 598, 2022.
[37] S. S. Kumar, S. D. Kumar, U. Magarajan, and S. Divya, "Study of mechanical and wear behaviour of AA5083 graphene reinforced composites," *Kovove Materialy-Metallic Materials*, vol. 60, no. 2, pp. 121–129, 2022.